Level density of 2^+ states in ^{40}Ca from high-energy-resolution (p,p') experiments

I. Usman,[1,2] Z. Buthelezi,[1] J. Carter,[2] G. R. J. Cooper,[3] R. W. Fearick,[4] S. V. Förtsch,[1] H. Fujita,[1,2,*] Y. Kalmykov,[5] P. von Neumann-Cosel,[5,†] R. Neveling,[1] I. Poltoratska,[5] A. Richter,[5,6] A. Shevchenko,[5] E. Sideras-Haddad,[2] F. D. Smit,[1] and J. Wambach[5]

[1]*iThemba LABS, P.O. Box 722, Somerset West 7129, South Africa*
[2]*School of Physics, University of the Witwatersrand, Johannesburg 2050, South Africa*
[3]*School of Earth Sciences, University of the Witwatersrand, Johannesburg 2050, South Africa*
[4]*Department of Physics, University of Cape Town, Rondebosch 7700, South Africa*
[5]*Institut für Kernphysik, Technische Universität Darmstadt, D-64289 Darmstadt, Germany*
[6]*ECT*, Villa Tambosi, I-38123 Villazzano (Trento), Italy*

(Received 6 October 2011; published 28 November 2011)

The level density of 2^+ states in ^{40}Ca has been extracted in the energy region of the isoscalar giant quadrupole resonance from a fluctuation analysis of high-energy-resolution (p, p') data taken at incident energies of 200 MeV at the K600 magnetic spectrometer of iThemba LABS, South Africa. Quasifree-scattering cross sections were calculated to estimate their role as a background contribution to the spectra and found to be small. The shape of the background was determined from the discrete wavelet transform of the spectra using a biorthogonal wavelet function normalized at the lowest particle separation threshold. The experimental results are compared to widely used phenomenological and microscopic models.

DOI: 10.1103/PhysRevC.84.054322 PACS number(s): 21.10.Ma, 25.40.Ep, 24.30.Cz, 27.40.+z

I. INTRODUCTION

Level densities are fundamental quantities in the description of many-body systems [1]. Besides their importance as a basic nuclear structure property, it is well known that, through the statistical model of nuclear reactions, level densities have a strong impact on the results of calculations of other nuclear physics observables. This is particularly so for thermonuclear rates in nucleosynthesis models [2,3], in fission and fusion reactor design [4], and for the derivation of γ-strength functions from the decay of highly excited nuclei [5].

Experimental information on level densities is largely confined to low excitation energies, where knowledge of the excited states is rather complete, and just above the particle emission thresholds, where resonance spacings can be determined from capture reactions. Some information on level densities at higher excitation energies has been extracted from the analysis of Ericson fluctuations (see, e.g., Ref. [6] and references therein). Here we present results derived from high-energy-resolution measurements of scattering cross sections in the energy region of giant resonances. The method is based on a fluctuation analysis of the spectra [7,8] and has been successfully applied recently to giant resonance data for a variety of modes like Gamow-Teller (GT) and electric and magnetic quadrupole resonances [9,10]. It provides not a total but a spin- and parity-resolved level density determined by the quantum numbers of the investigated resonance. In the present work we study 2^+ states in ^{40}Ca from an analysis of high-energy-resolution (p, p') data taken at an incident energy of 200 MeV and for kinematics favoring population of the isoscalar giant quadrupole resonance (ISGQR) at the K600 magnetic spectrometer of iThemba LABS, South Africa [11].

A prerequisite for the method is the decomposition of the spectra into the part stemming from excitation of the ISGQR and any background. The latter may contain contributions from the experimental instrumentation, excitation of other multipoles, and other physical processes. For hadronic probes quasifree scattering must be considered as a source of background in the energy region above the lowest particle threshold, where the giant resonance strength resides. For the case of proton scattering considered here, models have been developed in the framework of the distorted wave impulse approximation (DWIA) and have been shown to be quite successful at incident energies up to a few hundred mega–electron volts [12]. Alternatively, the shape of the underlying background can be determined in a largely model-independent way using a discrete wavelet analysis [9].

The results are compared to theoretical level densities from approaches based on the phenomenological back-shifted Fermi gas model (BSFG) [13,14] and microscopic Hartree-Fock-Bardeen-Cooper-Schrieffer (HF-BCS) [15] and Hartree-Fock-Bogolyubov (HFB) [16] calculations. Experimental tests of the latter are of particular interest, as the predictive power of the BSFG for extrapolations to exotic nuclei is limited. Thus, network calculations of the astrophysical r process typically depend on microscopic level densities [3]. Nuclei with shell closures are particularly difficult to describe in phenomenological models because their parameters do not follow the smooth systematics as a function of basic quantities like mass number observed otherwise, and ^{40}Ca is thus special because of its doubly magic nature. In addition, because of the weakening of low-energy quadrupole vibrations in doubly magic nuclei, it also provides a test of vibrational enhancement factors in microscopic calculations.

*Present address: Research Center for Nuclear Physics, Osaka University, Ibaraki, Osaka 567-0047, Japan.
†vnc@ikp.tu-darmstadt.de

II. EXPERIMENT

The fine structure of the ISGQR in medium-mass and heavy nuclei has been investigated with high-resolution (p, p') scattering at iThemba LABS with the aim of extracting information about their dominant decay processes [17,18]. Recently, these studies have been extended to the low-mass region $12 \leqslant A \leqslant 40$ [19,20]. The present work focuses on the case of ^{40}Ca where highly fragmented $E2$ strength has been observed with a variety of probes including inelastic electron [21], proton [22], and α [23] scattering.

In the experiment a 200-MeV proton beam produced by the Separated Sector Cyclotron of iThemba LABS was inelastically scattered off a natural Ca target (areal density 3.0 mg/cm^2) and detected with the K600 magnetic spectrometer. In order to achieve a high energy resolution the beam dispersion was matched to the spectrometer, leading to a resolution $\Delta E = 35$–40 keV (full width at half-maximum; FWHM). Data were taken at scattering angles $\theta_{\rm Lab} = 7^\circ$, 11°, and 15° chosen to lie below, at, and above the maximum of the cross sections for $\Delta L = 2$ transitions populating the ISGQR. The momentum acceptance of the spectrometer allowed to cover excitation energies between 6 and 30 MeV in ^{40}Ca with a single field setting. Details of the data analysis are described elsewhere [19]. The resulting spectra are displayed in Fig. 1.

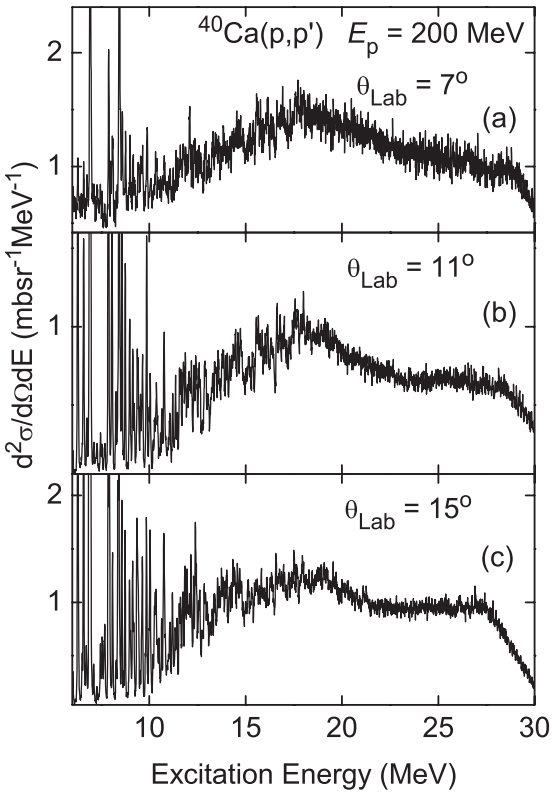

FIG. 1. Excitation energy spectra for ^{40}Ca for $E_x \approx 6$–30 MeV at scattering angles $\theta_{\rm Lab} = 7^\circ$, 11°, and 15°. Note that the ISGQR is expected to be most strongly excited at $\theta_{\rm Lab} = 11^\circ$. See also Ref. [20].

The spectra, already discussed in Ref. [20], exhibit a broad bump (roughly between 12 and 22 MeV) peaking around 18 MeV for scattering angles $\theta_{\rm Lab} = 11^\circ$ and 15°. It is associated with excitation of the ISGQR. Below $E_x \simeq 10$ MeV, many strong discrete transitions are visible with varying angular momentum transfer. Pronounced fine structure is visible in the excitation region of the ISGQR up to about 20 MeV. The intermediate structure with peaks around 12, 14, 16, 17 and 18 MeV is consistent with previous experimental results [21–23]. At the smaller scattering angle $\theta_{\rm Lab} = 7^\circ$, the maximum cross section is shifted to about 17 MeV, and the fine structure changes considerably, indicating the presence of other multipoles. Arguments for the predominance of quadrupole excitations in the 11° and 15° spectra including a cross-correlation analysis have been presented in Ref. [20].

III. BACKGROUND DETERMINATION

As pointed out above, knowledge of background in the spectra not related to population of the ISGQR is mandatory for extraction of the level densities. The background can have contributions from other multipoles excited, quasifree scattering, and the experimental instrumentation. The latter has been shown to be negligible in the present case [19]. Quasifree scattering dominates the cross sections in intermediate-energy proton scattering at excitation energies above the giant-resonance region [12] and could thus contribute substantially to the data investigated here. Their relevance is estimated from DWIA model calculations, which have been validated against a variety of data for incident proton energies up to 200 MeV (see, e.g., Refs. [24–26]). Alternatively, the shape of the underlying background can be determined in a largely model-independent way using a wavelet analysis of the discrete wavelet transform (DWT) of the spectra [9]. This method has been successfully applied [10] to proton scattering spectra of ^{58}Ni and ^{90}Zr in the energy region of the ISGQR [18].

A. Quasifree-scattering calculations

The code THREEDEE [27] was used for calculation of quasifree nucleon knockout contributions from the reactions ^{40}Ca$(p, 2p)^{39}$K and ^{40}Ca$(p, pn)^{39}$Ca at an incident proton energy of 200 MeV. The DWIA is used to determine the contribution owing to quasifree proton and neutron knockout in the inclusive proton-scattering reaction based on the assumption of a simple quasifree projectile-nucleon interaction. Such reactions indeed contribute to the background underlying the ISGQR in ^{40}Ca as demonstrated in earlier studies of ^{40}Ca$(p, p'p)$, ^{48}Ca$(p, p'n)$, and ^{40}Ca$(p, p'\alpha)$ angular correlations [22,25].

The low-energy proton and neutron optical-potential parameters used for description of the distorted outgoing waves are given in Ref. [28]. Optical potential parameters used for generating distorted waves of the high-energy incoming proton and its subsequent quasifree-scattering outgoing proton stem from the energy- and mass-dependent parametrization

of Ref. [29] extrapolated to energies of up to 200 MeV. The Woods-Saxon well radius and diffuseness parameters for calculation of proton and neutron bound-state wave functions were taken from Elton and Swift [30]. In order to perform the integration over the kinematics of the knocked-out particle, the recoil momentum was chosen to be less than 200 MeV/c to determine the range of the quasifree-scattering primary angles at each proton energy. The program QUASTA [31] was used for kinematic calculations. Contributions to the cross sections owing to the quasifree process were obtained in terms of the sum of the cross sections for knockout from the $1d_{3/2}$, $2s_{1/2}$, and $1d_{5/2}$ states for both protons and neutrons, with spectroscopic factors taken from Ref. [32] for proton and Refs. [33,34] for neutron states, except for the neutron $1d_{3/2}$ shell, where the shell-model limit of 4.0 was used. Calculations were performed within a range of excitation energies $E_x = 10$–30 MeV, corresponding to ejectile energies $E'_p \simeq 190$–170 MeV, respectively. In previous work at a lower incident energy, it was found that the contribution owing to the ^{40}Ca$(p, p'\alpha)$ reaction was very small [22,25]. Test calculations confirmed this for the present case, and therefore, quasifree $(p, p'\alpha)$ scattering was neglected.

Results of the calculations are shown in Fig. 2 for $\theta_{\rm Lab} = 11^\circ$ by way of example. Because of the much lower proton emission threshold ($S_p = 8.3$ MeV), the $(p, 2p)$ reaction dominates up to $E_x \approx 25$ MeV, while contributions from the (p, pn) reaction are comparable at higher excitation energies but small in the energy region of the ISGQR because of the high neutron separation energy ($S_n = 15.6$ MeV). In Fig. 3, the predicted total quasifree cross section is compared with the measured ^{40}Ca(p, p') cross sections. It can be seen that the quasifree contribution is relevant only for excitation energies $E_x > 20$ MeV, and even at 25 MeV it represents not more than about half the experimental value. The quasifree parts of the cross sections at other scattering angles are comparable [19]. Clearly, the quasifree process contributes little in the excitation energy region of interest and thus cannot provide a good approximation of the background.

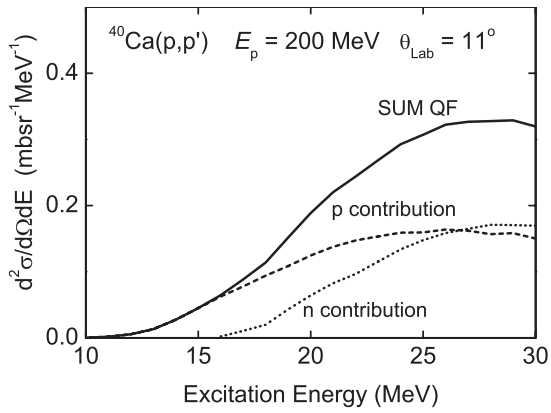

FIG. 2. Results of the DWIA calculations for quasifree reaction cross sections (SUM QF) of the ^{40}Ca(p, p')reaction at $E_p = 200$ MeV and $\theta_{\rm Lab} = 11^\circ$ (solid line) and their decomposition into contributions from $(p, 2p)$ (dashed line) and (p, pn) (dotted line) reactions.

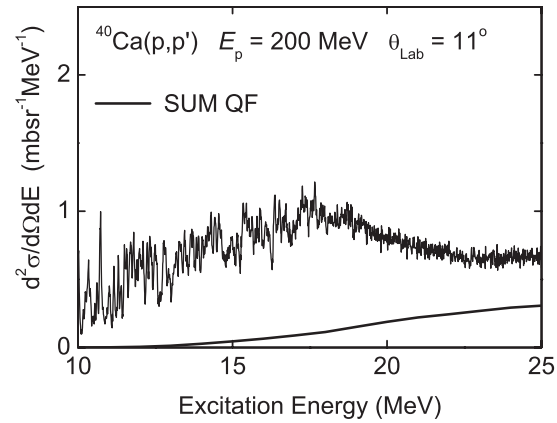

FIG. 3. Quasifree background contribution (SUM QF) to the spectrum of the ^{40}Ca(p, p') reaction at $E_p = 200$ MeV and $\theta_{\rm Lab} = 11^\circ$.

B. Discrete wavelet transform

In high-energy resolution spectra dominated by a single giant resonance, the shape of the underlying background can be determined in a model-independent way using a wavelet analysis of the DWT of the spectrum [9]. A comprehensive description of the application of wavelet analysis to high-resolution nuclear spectra can be found in Ref. [35]. Here, we reiterate only a few basic facts necessary to understand the specific approach to background determination. The wavelet analysis is performed by folding the original spectrum $\sigma(E)$ with a wavelet function Ψ, resulting in wavelet coefficients

$$C(E_x, \delta E) = \frac{1}{\sqrt{\delta E}} \int \sigma(E) \Psi\left(\frac{E_x - E}{\delta E}\right) dE. \qquad (1)$$

The parameters (excitation energy E_x and scale δE) can be varied in continuous (adjustable to the specfic problem) or discrete ($\delta E = 2^j$, $E_x = k\delta E$, $j, k = 1, 2, 3 \ldots$) steps leading to a continuous wavelet transform (CWT) or a DWT of the original spectrum, respectively. The CWT can be used to extract scales characterizing the fine structure of the spectra [17,18,20,36]. The DWT, while limited in scale resolution, allows us to reassemble the original signal from the wavelet coefficients.

The present application, furthermore, utilizes the property of vanishing moments fulfilled by many wavelet functions; namely,

$$\int E^n \Psi(E)\, dE = 0, \quad n = 0, 1, \ldots, m. \qquad (2)$$

When Eq. (2) holds, any nonresonant background in the spectrum, whether of physical or experimental nature, does not contribute to the wavelet coefficients as long as it can be approximated by a polynomial function of order m. In the present analysis the biorthogonal family of mother wavelets BIOR$Nr.Nd$ was used, where Nr indicates the nth vanishing moment with a polynomial function of order $n - 1$, while Nd represents the level of decomposition [37]. Examples of BIOR wavelets are shown in Fig. 4.

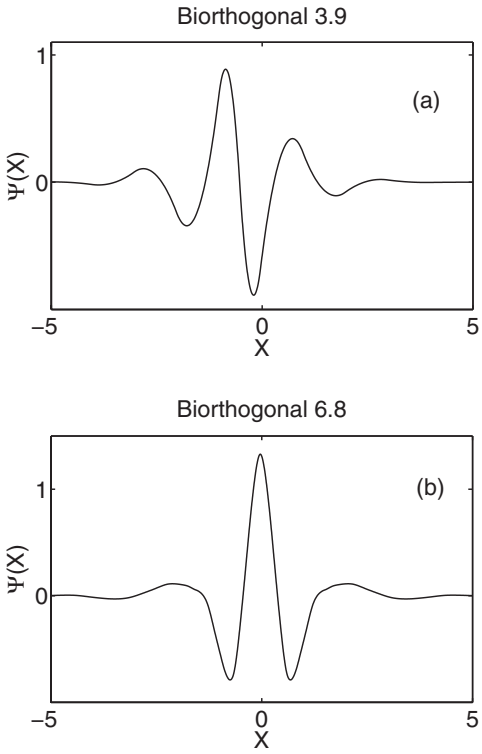

FIG. 4. Examples of wavelet functions used in the present analysis. (a) BIOR3.9 wavelet. (b) BIOR6.8 wavelet.

The DWT can be viewed as an iterative decomposition in the form of low-pass and high-pass filtering of the data into a sequence of approximations (A_j) and details (D_j) with increasing scale δE_j. At each level of decomposition, $A_j + D_j = A_{j-1}$. The approximations are the filtered signals, which provide the nonresonant background at the given range of scale values, while the details obtained from the wavelet coefficients provide the part of the signal that was removed in the filtering process at that level. Application of the DWT to the spectrum measured at $\theta_{\rm Lab} = 11^\circ$ is shown in Fig. 5. The distributions of details indicate that scales between about 100 keV and 1 MeV ($D_4 - D_7$) contribute most to the fine structure in the energy region of the ISGQR. This is fully consistent with a wavelet analysis based on the CWT [20], which finds maxima of the power spectrum of the wavelet coefficients (so-called characteristic scales) at values of 150, 240, 460 keV, and 1.05 MeV.

At some level of decomposition the largest physical scale in the spectrum, *viz.*, the width of the ISGQR, is reached in the approximations ($A9$ in the present example). This is demonstrated in Fig. 6, where the the spectra measured at 11° and 15° are compared to the approximations $A9$ of the respective DWT analysis shown as dashed-dotted lines. The main structure between 10 and 20 MeV associated with the ISGQR is well described in both cases. Structures at even larger scales (see approximation $A10$ in Fig. 5) are thus associated with the background.

The impact of a variation of the number of vanishing moments in the DWT analysis is also demonstrated in Fig. 6, where the background shapes $A10$ deduced with different biorthogonal wavelet functions are compared. While the energy dependence extracted with BIOR3.9 differs, the spectral shapes are very similar for larger numbers of vanishing moments. The results discussed in the following are based on the application of a BIOR6.8 wavelet. A fine-tuning of the resulting background is then carried out by shifting of the $A10$ form in the vertical direction in order to satisfy the experimental condition that the spectrum is background-free below the proton threshold.

IV. LEVEL DENSITY OF 2^+ STATES

A. Fluctuation analysis

In this section, the level density of 2^+ states in ^{40}Ca extracted by means of a self-consistent procedure based on a fluctuation analysis [7] in the excitation energy interval between 10 and 20 MeV is discussed. As a starting point, the measured excitation energy spectrum for ^{40}Ca(p, p') at $\theta_{\rm Lab} = 11^\circ$, together with the background deduced from the DWT analysis with a BIOR6.8 wavelet (solid line), is shown in Fig. 7(a). The method discussed here is applicable in a region where $\langle\Gamma\rangle/\langle D\rangle \ll 1$ but $\langle D\rangle < \Delta E$. Here, $\langle\Gamma\rangle$ represents the mean level width, $\langle D\rangle$ is the mean level spacing, and ΔE is the experimental energy resolution. The first step of the fluctuation analysis is a subtraction of the nonresonant background determined as described in the previous section from the spectrum. Then a smoothing is performed using a Gaussian function with a width σ smaller than the experimental energy resolution ΔE in order to suppress contributions owing to statistical fluctuations. The resulting spectrum is called $g\,(E_{\rm x})$. This spectrum is again folded with a Gaussian, of a width $\sigma_>$ larger than the experimental energy resolution, in order to remove gross structures. The resulting spectrum, referred to as $g_>\,(E_{\rm x})$, is displayed in Fig. 7(b) and defines a mean value around which the original data fluctuate. The ratio of $g\,(E_{\rm x})$ to $g_>\,(E_{\rm x})$ is called the stationary spectrum, which fluctuates around unity as demonstrated in Fig. 7(c). It represents a direct measure of the local intensity fluctuations, which can be expressed in terms of an autocorrelation function of the spectrum

$$C\,(\epsilon) = \langle d\,(E_{\rm x})\,d\,(E_{\rm x}+\epsilon)\rangle, \tag{3}$$

where ϵ denotes the energy shift and the angle braces indicate averaging over a suitable energy interval. The value $C\,(\epsilon = 0) - 1$ is the variance.

This experimental autocorrelation function can be approximated by the analytical expression [7]

$$C\,(\epsilon) - 1 = \frac{\alpha\langle D\rangle}{2\Delta E\sqrt{\pi}} f\,(\epsilon, \Delta E, \sigma, \sigma_>)\,, \tag{4}$$

where the function f is normalized such that $f(\epsilon = 0) = 1$. From Eq. (4) it follows that the value of the autocorrelation function $[C\,(\epsilon) - 1]$ at $\epsilon = 0$, i.e., the variance of the stationary spectrum, is proportional to the mean level spacing $\langle D\rangle$. Thus, $\langle D\rangle$ can be extracted directly when the normalized variance α of the underlying spectral distributions is known. It is assumed that because of the high excitation energies, these can be approximated by the predictions of random matrix theory [38],

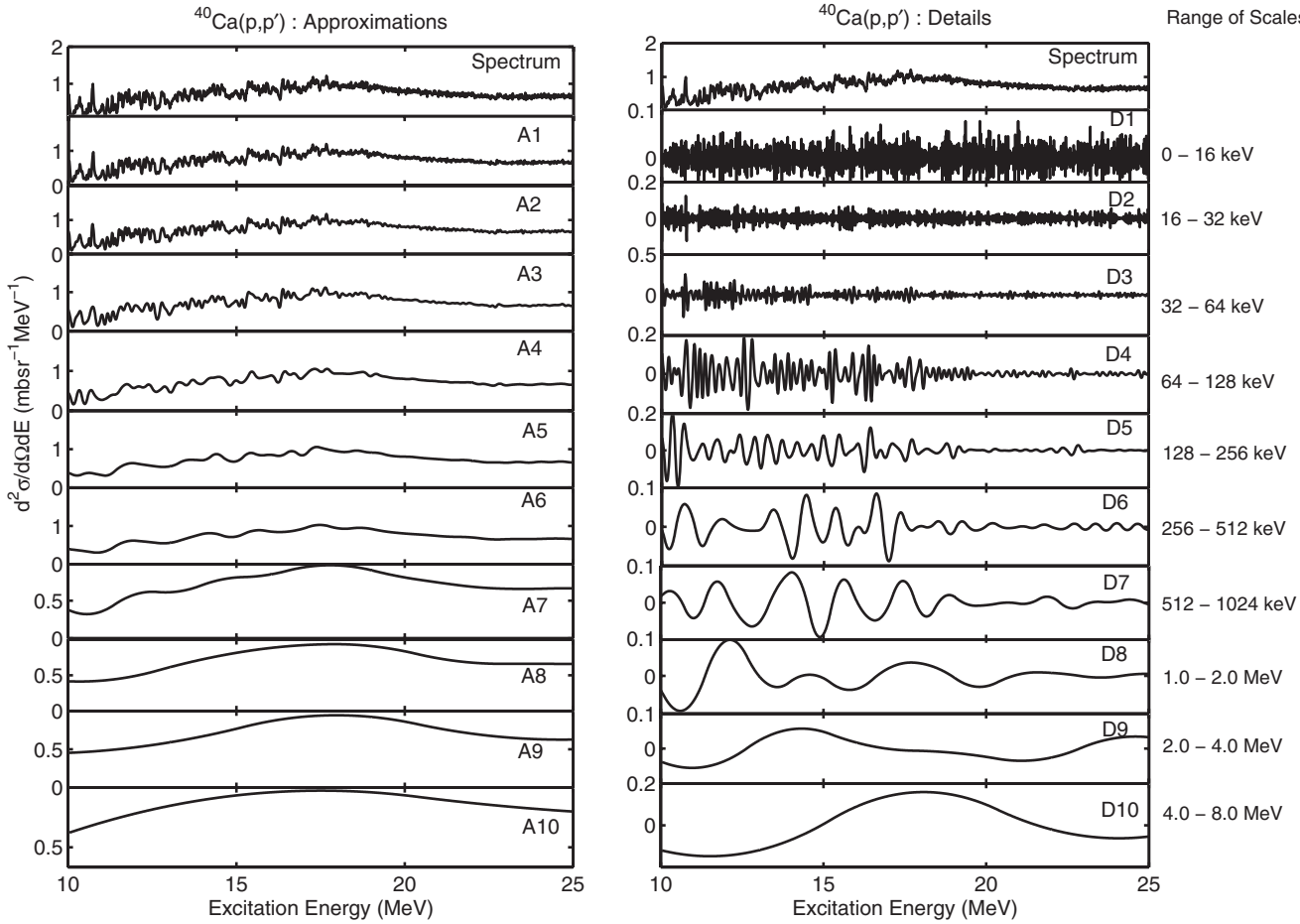

FIG. 5. DWT decomposition of the excitation energy spectrum of the ^{40}Ca(p, p') reaction measured at $E_p = 200$ MeV for $\theta_{\rm Lab} = 11^\circ$ into approximations Ai and details Di.

i.e., a Wigner distribution for the level spacing and a Porter-Thomas (PT) distribution for the intensities. If one assumes that the cross sections result from a single class of states, i.e., $J^\pi = 2^+$ states in the region of the ISGQR, then $\alpha = \alpha_{\rm Wigner} + \alpha_{\rm PT} = 2.237$. Figure 7(d) illustrates the autocorrelation functions for both the experimental data and the model. Because the ϵ dependence is contained in the function f, which depends on experimental parameters only, $\langle D \rangle$ is determined by the value of the autocorrelation function at $\epsilon = 0$.

B. Experimental results

The analysis requires a suitable interval length in order to keep finite-range-of-data errors [39] at an acceptable level. In the present case, 2-MeV intervals were chosen. The resulting level densities for the spectra measured at 11° and 15° are summarized in Table I. The results should be independent of the kinematics of the measurement, and indeed agreement between the values deduced from the two spectra within experimental uncertainties is obtained, confirming the correctness of the assumptions underlying their extraction. The uncertainties of the extracted level densities given in Table I were obtained by varying the input parameters of the autocorrelation function and the fluctuation analysis as well as the background subtraction method and repeating the analysis. The following contributions, assumed to be independent of each other, have been considered in the calculation of the experimental error bars.

(i) Smoothing parameters: A variation by ±10% leads to a 2% error contribution.

(ii) Range of the excitation energy interval: The analysis was repeated for interval sizes between 0.5 and 2 MeV. The corresponding uncertainty amounts to ±10%.

(iii) Variations of the normalized variances of the spacing and intensity distributions in Eq. (4): This owes to admixtures of states with another spin and/or parity and depends on the ratio of level densities and cross sections [40]. Asymptotically, for the spacing distribution one approaches a value $\alpha_s = 2 + 3N_1/N_2$, where N_1/N_2 denotes the cross-section ratio of the two multipoles. An upper limit of $N_1/N_2 = 0.1$ was assumed based on the arguments for a dominant excitation of the ISGQR in the spectra discussed in Ref. [20]. Variations in the variance of the intensity contribution can be neglected for small admixtures. Because α in Eq. (4) only increases for values $N_1/N_2 \neq 0$, the level density also increases, leading to a +13% error.

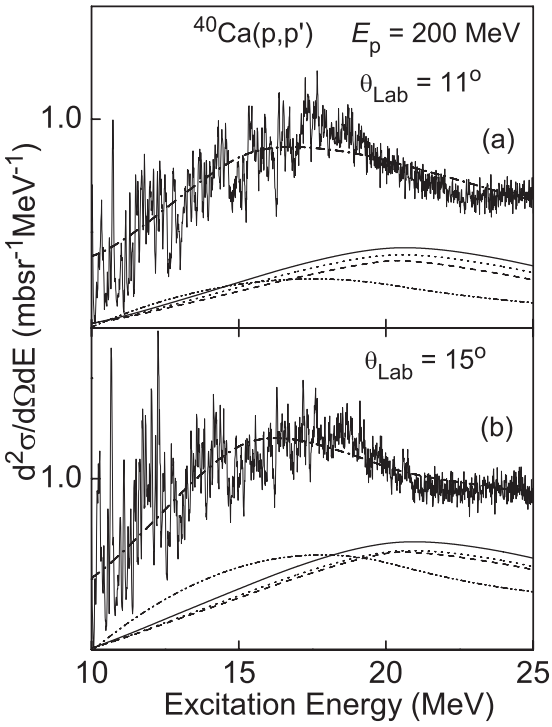

FIG. 6. Comparison of the spectrum of the ^{40}Ca(p, p') reaction measured at $E_p = 200$ MeV for (a) $\theta_{Lab} = 11^\circ$ and (b) $\theta_{Lab} = 15^\circ$ to approximation $A9$ (dashed-dotted lines) determined from the DWT (cf. Fig. 5). The shape of the ISGQR is well reproduced. The resulting background (approximation $A10$) is shown for different biorthogonal wavelet functions: BIOR6.8 (solid lines), BIOR5.5 (dotted lines), BIOR4.4 (dashed lines), and BIOR3.9 (dashed-doubly dotted lines).

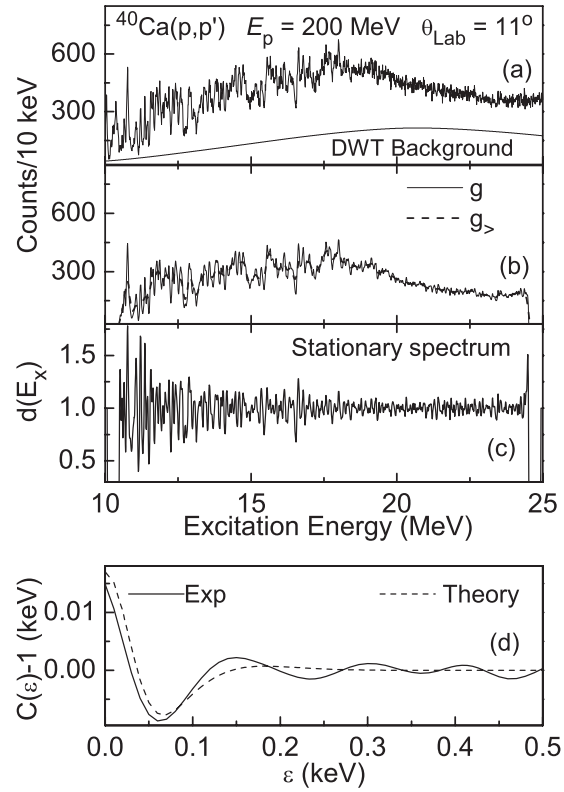

FIG. 7. Illustration of the autocorrelation analysis: (a) experimental ^{40}Ca(p, p') spectrum including background obtained with the use of the discrete wavelet transform; (b) background-subtracted smoothed spectra $g(E_x)$ and $g_>(E_x)$, respectively; (c) stationary fluctuating spectrum $d(E_x)$ obtained by dividing the two smoothed spectra; and (d) autocorrelation functions from experiment and Eq. (4), shown as the solid and dashed line, respectively.

(iv) Choice of wavelet functions: The variation between the different choices of the BIOR wavelets (Fig. 6) is taken as an estimate of the uncertainty of the background determination. Increasing the number of vanishing moments leads to larger backgrounds but approaching a constant magnitude and shape for the highest values used in the present analysis. The variation thus leads to a systematic reduction of the level densities reaching -17% for the 11° and -13% for the 15° spectrum, respectively.

C. Model comparison

Shown in Fig. 8 are the experimental level densities deduced from both spectra in comparison to model calculations. The theoretical results considered include the phenomenological back-shifted Fermi gas (BSFG) and microscopic models. Two sets of values were taken for the BSFG parameters Δ, the ground-state energy correction accounting for pairing and shell effects, and the level density parameter a describing the exponential increase with energy. Rauscher *et al.* [13] provide a fit to stable nuclei across the nuclear chart which is used for astrophysical network calculations of the s process, including extra parameters for an improvement of the description in local mass areas. von Egidy and Bucurescu [14] performed a global fit with parameters dependent on experimental masses only. The latter approach was recently improved by a modification of the spin-cutoff parameter [41], which is in accordance with shell-model Monte Carlo calculations [42]. A current microscopic approach is based on an HFB plus combinatorial model [43]. This was improved in Ref. [16] to include, beyond rotational, also vibrational degrees of freedom. We also show a comparison with HF-BCS model results [15].

TABLE I. Level density of 2^+ states in ^{40}Ca at various excitation energies E_x extracted from the (p, p') data at scattering angles $\theta_{Lab} = 11^\circ$ and 15°.

E_x (MeV)	Level density (MeV^{-1})	
	11°	15°
11	$17.5^{+2.9}_{-3.1}$	$18.1^{+3.0}_{-1.9}$
13	$64.1^{+10.6}_{-10.7}$	$57.3^{+9.5}_{-6.6}$
15	213^{+35}_{-38}	224^{+37}_{-32}
17	217^{+36}_{-43}	236^{+39}_{-37}
19	1007^{+166}_{-226}	705^{+116}_{-122}

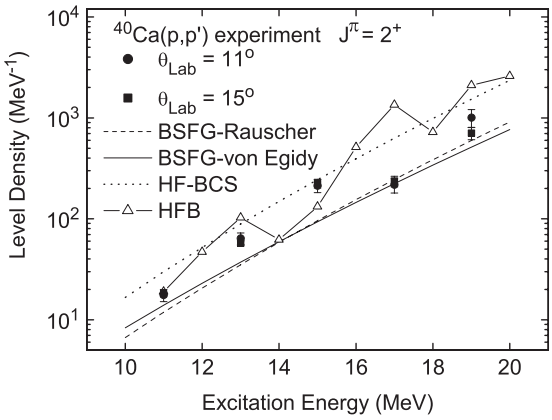

FIG. 8. Level density of 2^+ states in ^{40}Ca extracted from the (p, p') data (filled symbols) compared to model predictions: BSFG-Rauscher [13] (dashed line), BSFG–von Egidy [41] (solid line), HF-BCS [15] (dotted line), and HFB [16] (triangles; the connecting line is a guide for the eye only).

Both BSFG parametrizations provide very similar results for 2^+ states in ^{40}Ca in the excitation energy range considered, $E_x \simeq 10$–20 MeV. The corresponding level density parameter $a \approx 5.3\,\mathrm{MeV}^{-1}$, which is unusually low because of the double shell closure, provides a reasonable description of the energy dependence in the experimental results, but the magnitudes are about a factor of 2 too low. The energy dependence of the HF-BCS calculation is again very similar to the data and the BSFG results, but the predicted level densities are about 50% too high. Because an implicit assumption of all three models is the equipartition of states with positive and negative parity for a given spin, the theoretical results were divided by a factor of 2 for the comparison in Fig. 8.

The HFB model is capable of calculating level densities of states with given spin and parity and, furthermore, allows for deviations from the smooth energy dependence encoded within the BSFG and HF-BCS models by the microscopically generated distribution of single-particle states and collective enhancement factors. The data indeed indicate such fluctuations, similarly to findings in Ref. [10]. However, in detail, the correspondence of fluctuations around the average increase in the level densities extracted from the data and the HFB calculations is limited. For example, at $E_x = 17$ MeV the data find a local minimum, while the HFB result predicts a maximum. However, the absolute magnitude is reasonably described by the HFB calculations despite the fact that no renormalization (cf. Eq. (9) of Ref. [16]) to the experimental level scheme at low energy and neutron resonance spacings was included. The average energy dependence describes the data up to 15 MeV well but overpredicts the experimental results at higher excitation energies.

V. CONCLUSIONS AND OUTLOOK

The present work reports on the level density of 2^+ states in ^{40}Ca in the energy region of the ISGQR. It is extracted from high-energy resolution proton scattering spectra measured in kinematics favoring quadrupole transitions. The method is based on the analysis of cross-section fluctuations and thus is dependent on the highest possible energy resolution. The magnitude of the fluctuations is determined by an autocorrelation function and can be related to the average level spacing [7].

A crucial input into the analysis is the knowledge of background contributions to the measured excitation energy spectra. In the present work, these were determined by a decomposition of the spectrum with a discrete wavelet analysis described in Ref. [35] which was, for example, successfully applied [10] to experiments studying the ISGQR [17,18] and magnetic quadrupole resonance [44] in medium-heavy nuclei. Alternatively, the role of quasifree reactions as a background source was estimated but found to be small. The DWT analysis is largely model independent but depends on two assumptions, *viz.,* that the energy dependence of background contributions in the spectra can be approximated by a polynomial and that one excitation mode dominates the spectra. Based on the agreement of experimental level densities deduced for different kinematics, we conclude that these conditions are well fulfilled for the present case (for the latter point see also the discussion in Ref. [20]). The extracted level densities were compared to phenomenological BSFG and microscopic HF-BCS and HFB calculations. The excitation energy dependence is reasonably well described by the BSFG and HF-BCS models, but absolute values are either over- or underestimated. The HFB calculation provides the correct magnitude up to about 15 MeV but overestimates the experimental values at higher excitation energies.

The relevance of this new technique combining a fluctuation analysis of high-energy resolution spectra with a discrete wavelet decomposition to determine background components is twofold: because the method works best in the energy region where giant resonances dominate the cross sections, it provides experimental data on level densities for $E_x \approx 10$–30 MeV that are difficult to experimentally access otherwise, and it also provides information for states of specific spin and parity, thus allowing tests of the spin distribution models [41] and claims of a parity dependence of level densities [45] with significant astrophysical consequences [46,47]. Beyond the application to electric and magnetic quadrupole modes discussed so far, new facilities allowing for high-resolution 0° scattering experiments of hadronic beams [11,48] promise data for $\Delta L = 0$ and 1 natural-parity modes from α scattering [49,50] and proton scattering [51], respectively. Unnatural-parity states can be studied in backward-angle electron scattering [44,52] and charge-exchange reactions [9,53]. Systematic studies of spin- and parity-resolved level densities along these lines are in progress.

ACKNOWLEDGMENTS

We are indebted to J. L. Conradie and the accelerator crew at iThemba LABS for providing excellent proton beams. Useful discussions with S. Goriely are acknowledged. This work was supported by the National Research Foundation (South Africa) and by the Deutsche Forschungsgemeinschaft under Contract Nos. SFB 634 and NE 679/2-2.

[1] J. R. Huizenga and L. G. Moretto, Annu. Rev. Nucl. Sci. **22**, 427 (1972).
[2] T. Rauscher and F.-K. Thielemann, At. Data Nucl. Data Tables **75**, 1 (2000).
[3] M. Arnould, S. Goriely, and K. Takahashi, Phys. Rep. **450**, 97 (2007).
[4] R. Capote *et al.*, Nucl. Data Sheets **110**, 3107 (2009).
[5] A. C. Larsen *et al.*, Phys. Rev. C **83**, 034315 (2011).
[6] S. M. Grimes, J. Nucl. Sci. Technol. Suppl. **2**, 709 (2002).
[7] P. G. Hansen, B. Jonson, and A. Richter, Nucl. Phys. A **518**, 13 (1990).
[8] S. Müller, F. Beck, D. Meuer, and A. Richter, Phys. Lett. B **113**, 362 (1982).
[9] Y. Kalmykov *et al.*, Phys. Rev. Lett. **96**, 012502 (2006).
[10] Y. Kalmykov, C. Özen, K. Langanke, G. Martínez-Pinedo, P. von Neumann-Cosel, and A. Richter, Phys. Rev. Lett. **99**, 202502 (2007).
[11] R. Neveling *et al.*, Nucl. Instrum. Methods Phys. Res. Sec. A **654**, 29 (2011).
[12] F. T. Baker *et al.*, Phys. Rep. **289**, 235 (1997).
[13] T. Rauscher, F. K. Thielemann, and K.-L. Kratz, Phys. Rev. C **56**, 1613 (1997).
[14] T. von Egidy and D. Bucurescu, Phys. Rev. C **72**, 044311 (2005).
[15] P. Demetriou and S. Goriely, Nucl. Phys. A **695**, 95 (2001).
[16] S. Goriely, S. Hilaire, and A. J. Koning, Phys. Rev. C **78**, 064307 (2008).
[17] A. Shevchenko *et al.*, Phys. Rev. Lett. **93**, 122501 (2004).
[18] A. Shevchenko *et al.*, Phys. Rev. C **79**, 044305 (2009).
[19] I. Usman, Ph.D. thesis, University of the Witwatersrand, 2009.
[20] I. Usman *et al.*, Phys. Lett. B **698**, 191 (2011).
[21] H. Diesener *et al.*, Phys. Rev. Lett. **72**, 1994 (1994); Nucl. Phys. A **696**, 293 (2001).
[22] K. Schweda *et al.*, Phys. Lett. B **506**, 247 (2001).
[23] K. van der Borg, M. N. Harakeh, and A. van der Woude, Nucl. Phys. A **365**, 243 (1981); F. Zwarts, A. G. Drentje, M. N. Harakeh, and A. Van Der Woude, *ibid.* **439**, 117 (1985).
[24] A. A. Cowley, J. V. Pilcher, J. J. Lawrie, and D. M. Whittal, Phys. Rev. C **40**, 1950 (1989).
[25] J. Carter *et al.*, Phys. Rev. C **63**, 057602 (2001).
[26] R. Neveling, A. A. Cowley, G. F. Steyn, S. V. Förtsch, G. C. Hillhouse, J. Mano, and S. M. Wyngaardt, Phys. Rev. C **66**, 034602 (2002).
[27] N. S. Chant, THREEDEE, University of Maryland (1998) (unpublished).
[28] F. D. Becchetti and G. W. Greenlees, Phys. Rev. **182**, 1190 (1969).
[29] P. Schwandt, H. O. Meyer, W. W. Jacobs, A. D. Bacher, S. E. Vigdor, M. D. Kaitchuck, and T. R. Donoghue, Phys. Rev. C **26**, 55 (1982).
[30] L. R. B. Elton and A. Swift, Nucl. Phys. A **94**, 52 (1967).
[31] QUASTA, a three-body kinematics computer code developed at iThemba LABS (unpublished).
[32] L. Antonuk, P. Kitching, C. A. Miller, D. A. Hutcheon, W. J. McDonald, G. C. Neilson, W. C. Olsen, and A. W. Stetz, Nucl. Phys. A **370**, 389 (1981).
[33] J. W. Watson, M. Ahmad, D. W. Devins, B. S. Flanders, D. L. Friesel, N. S. Chant, P. G. Roos, and J. Wastell, Phys. Rev. C **26**, 961 (1982).
[34] M. Ahmad, J. W. Watson, D. W. Devins, B. S. Flanders, D. L. Friesel, N. S. Chant, P. G. Roos, and J. Wastell, Nucl. Phys. A **424**, 92 (1984).
[35] A. Shevchenko, J. Carter, G. R. J. Cooper, R. W. Fearick, Y. Kalmykov, P. von Neumann-Cosel, V. Yu. Ponomarev, A. Richter, I. Usman, and J. Wambach, Phys. Rev. C **77**, 024302 (2008).
[36] I. Petermann, K. Langanke, G. Martínez-Pinedo, P. von Neumann-Cosel, F. Nowacki, and A. Richter, Phys. Rev. C **81**, 014308 (2010).
[37] The Mathworks, Inc., Matlab, the Language of Technical Computing, Version 7.2.0.232 (R2006) (1984–2006).
[38] H. A. Weidenmüller and G. E. Mitchell, Rev. Mod. Phys. **81**, 539 (2009).
[39] A. Richter, in *Nuclear Spectroscopy and Reactions*, part B, edited by J. Cerny (Academic Press, New York, 1974), p. 343.
[40] G. Kilgus, G. Kühner, S. Müller, A. Richter, and W. Knüpfer, Z. Phys. A **326**, 41 (1987).
[41] T. von Egidy and D. Bucurescu, Phys. Rev. C **80**, 054310 (2009).
[42] Y. Alhassid, S. Liu, and H. Nakada, Phys. Rev. Lett. **99**, 162504 (2007).
[43] S. Hilaire and S. Goriely, Nucl. Phys. A **779**, 63 (2006).
[44] P. von Neumann-Cosel *et al.*, Phys. Rev. Lett. **82**, 1105 (1999).
[45] Y. Alhassid, G. F. Bertsch, S. Liu, and H. Nakada, Phys. Rev. Lett. **84**, 4313 (2000).
[46] H. Loens, K. Langanke, G. Martínez-Pinedo, T. Rauscher, and F.-K. Thielemann, Phys. Lett. B **666**, 395 (2008).
[47] L. Huther, H. P. Loens, G. Martínez-Pinedo, and K. Langanke, Eur. Phys. J. A **47**, 10 (2011).
[48] A. Tamii *et al.*, Nucl. Instrum. Methods Phys. Res. Sect. A **605**, 3 (2009).
[49] S. Brandenburg, R. De Leo, A. G. Drentje, M. N. Harakeh, H. Sakai, and A. van der Woude, Phys. Lett. B **130**, 9 (1983).
[50] H. J. Lu, S. Brandenburg, R. De Leo, M. N. Harakeh, T. D. Poelhekken, and A. van der Woude, Phys. Rev. C **33**, 1116 (1986).
[51] A. Tamii *et al.*, Phys. Rev. Lett. **107**, 062502 (2011).
[52] C. Lüttge *et al.*, Nucl. Instrum. Methods Phys. Res. Sec. A **366**, 325 (1995).
[53] H. Fujita *et al.*, Phys. Rev. C **75**, 034310 (2007).